applied optics

Low-repetition rate femtosecond laser writing of optical waveguides in water-white glass slides

H. E. Lazcano and G. V. Vázquez*

Centro de Investigaciones en Óptica, Loma del Bosque 115, Lomas del Campestre, C.P. 37150 León, Gto., Mexico
*Corresponding author: gvvazquez@cio.mx

Received 15 January 2016; revised 6 March 2016; accepted 15 March 2016; posted 16 March 2016 (Doc. ID 257624); published 15 April 2016

Energy dose ranges for fabrication of subsurface and ablated ridge waveguides were defined using a low repetition rate femtosecond laser. The waveguides were written along the width of water-white glass slides. The buried waveguides written between 0.23 and 0.62 μJ/μm^3 energy dose show strong guidance at 633 nm, reaching in the best cases propagation losses of 0.7 dB/cm. Meanwhile, the ridge waveguides were fabricated between 2.04 and 31.9 μJ/μm^3, with a best case of 3.1 dB/cm. Outcomes of this study are promising for use in the manufacturing of sensing devices.

OCIS codes: (130.2755) Glass waveguides; (140.7090) Ultrafast lasers; (230.7380) Waveguides, channeled.

http://dx.doi.org/10.1364/AO.55.003268

1. INTRODUCTION

Nowadays femtosecond laser micromachining is a technique that has been consolidated in the manufacture of optical waveguide structures because it has outstanding advantages such as the fabrication of three-dimensional photonic structures on or inside a transparent material [1–5] with short processing times and without the use of photomasks and additional chemical processes, allowing rapid prototyping of devices. The process by which the optical energy is transferred to the material is called laser-induced optical breakdown [6]. This energy transfer causes ionization of a large number of electrons, which in turn can cause permanent material modification by transferring energy to the lattice. In transparent materials the energy of a single photon cannot be absorbed, so the material must simultaneously absorb more than one photon. For nonlinear absorption to occur, the electric field strength in the laser pulse must be approximately equal to the electric field that binds the valence electrons in atoms. To achieve such high electric field strengths it is necessary to focus the light tightly. The tight focusing and the nonlinear nature of the absorption make it possible to confine the absorption to the focal volume over or inside the bulk of the material. The result is a localized deposition of energy, which later turns into thermal energy, causing the material to undergo a structural modification, leaving behind a localized permanent change in the index of refraction.

Two different regimes of femtosecond laser writing can be classified depending on the relationship between the repetition pulse rate and the thermal diffusion time. For the low repetition rate regime, the material modification is produced by individual pulses and the processing speed is relatively slow [7,8] around or less than 500 μm/s; for the high repetition rate regime, the time between successive pulses is shorter than the thermal diffusion time, resulting in a heat accumulation in the focal volume during laser processing [4,9]. This gives faster processing speed and symmetric cross section due to isotropic heat diffusion. On the other hand, according with [10], we report results on the fabrication of two different kinds of channel waveguides based on type I and II structures, through the low repetition rate regime. The proposed waveguide based on the type I structure is also called the directly written waveguide [11]. In this particular case, the femtosecond (fs) laser induces a positive refractive index change in the irradiated focal volume, which becomes the waveguide core. Additionally, the proposed ridge waveguide is based on the type II structure. In this configuration the high-intensity fs laser beam removes material from the surface and the written region becomes the border of the waveguide. The thermal effects induce a refractive index increase in the region between these boundaries; therefore, this region becomes the core. Hence to manufacture a waveguide with this configuration two tracks are required. Figure 1 shows the schematic representation of the fabrication of the proposed waveguides base on type I and type II structures.

Nowadays, developments based on active materials for the production of waveguides of different configurations are known. These waveguides have been used for laser and nonlinear applications [11–14]. Another trend is the combination of techniques to improve the performance of the waveguides or achieve more efficient structures. On the other hand, the development of waveguides in glass substrates, such as BK7, fused silica or SF10, has exhibited a great advance [15–17]. This work aims at the development of structures based on more affordable materials. We are interested in the fabrication of

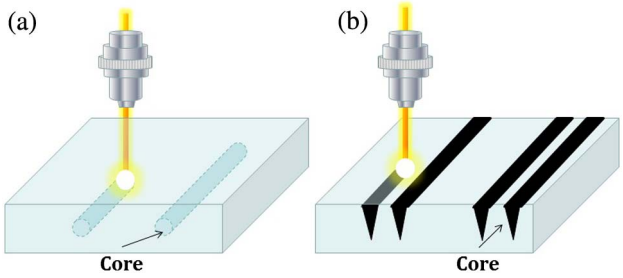

Fig. 1. Schematic representation of the fabricated waveguides. (a) Directly written waveguide based on the type I structure and (b) ridge waveguide based on the type II structure.

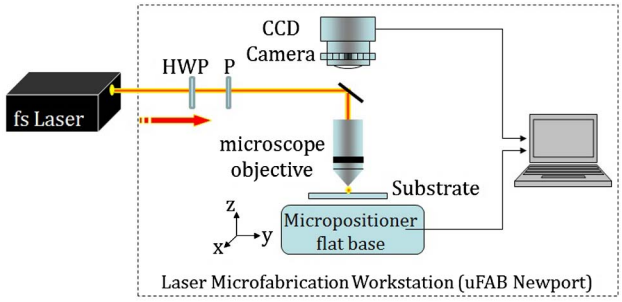

Fig. 2. Schematic representation of the experimental setup used for writing the waveguides.

channel waveguides that could be used in the design of optochemical sensing devices.

2. EXPERIMENTAL DETAILS

Straight channel waveguides were fabricated in water-white glass slides (Corning 2947B), using a low repetition rate (1 kHz) ultrafast Libra Coherent laser that has a central wavelength at 800 nm and produces 50 fs pulses. To manufacture the waveguides a laser microfabrication workstation (uFAB Newport) was used. The laser system used includes amplification, therefore power is greater than needed. Accordingly, a variable attenuation of laser light is possible through the use of a rotating half-wave plate (HWP) and fixed polarizer (P). Water-white glass, also called low-iron soda lime, is created by using high-quality grades of silica sand that are virtually free of iron oxides. This results in a transparent glass that has higher transmission characteristics compared to normal soda lime [18]; however, it remains very affordable and easily accessible. The incident laser beam is directed toward the uFAB workstation, where the HWP and P attenuate the laser beam power. After that a periscopic arrangement drives the laser beam to a microscope objective where it is finally focused over or inside the glass sample to write waveguides. The glass slide (1.1 cm width, 2.25 cm length, and 0.1 cm thickness), is mounted horizontally over a three-axis motorized flat base, which is part of the uFAB workstation. The glass substrate is translated perpendicular to the direction of the laser beam. It is possible to set the following fabrication parameters: base translation speed, acceleration, laser power, length, and distribution of the laser writing. Additionally, the workstation includes a CCD camera to observe the process. Experiments were carried out varying some of these parameters and also with three different microscope objectives (10×, 20×, and 40×, numerical apertures of 0.25, 0.4, and 0.65, respectively). The experimental setup is schematically shown in Fig. 2.

Although various parameters are controlled, to obtain homogeneous and replicable structures, the laser beam focus must be adjusted and replicated by the person who manufactures the waveguides, since it is not always clear when the focus is optimal. This is especially critical for the fabrication of ridge waveguides. The appearance of the beam depends on several factors, including characteristics of the camera, lighting, beam power, writing speed, type and flatness of the substrate, microscope objective, and focus. As an example, a sequence of different focusing is shown in Fig. 3. The focus shapes that are recommended for writing ridge waveguides correspond only to Figs. 3(b) and 3(c) (i.e., focus on the surface).

To accomplish the analysis, the input and output surfaces of the waveguides were polished; the process is described in [19]. The characterization of the waveguides was carried out using a XYZ micropositioner system (Newport 561D) and a 10× microscope objective in order to couple 633 nm light (He–Ne JDS Uniphase Laser) into the waveguide. To assess the waveguide, the output light was collimated with a 20× microscope objective. To determine the coefficient of propagation losses (α) the method described in [20] was adopted. This method uses Eq. (1) to calculate α [dB/cm], where L is the length of the waveguide, T_g is the transmittance of the waveguide, T_F is the Fresnel transmission coefficient at the output of the waveguide, and η_{ac} is the coupling loss coefficient:

$$\alpha = -\frac{10}{L}\,\mathrm{Log}_{10}\frac{T_g}{\eta_{ac}T_F}. \tag{1}$$

The input and output laser beam power and diameter were measured in every waveguide to feed Eq. (1). The power was measured with a power meter (Thorlabs PM100D) and the laser beam and mode dimensions with a CCD camera (Thorlabs BC106-VIS). The experimental setup for calculating α is schematically shown in Fig. 4(a).

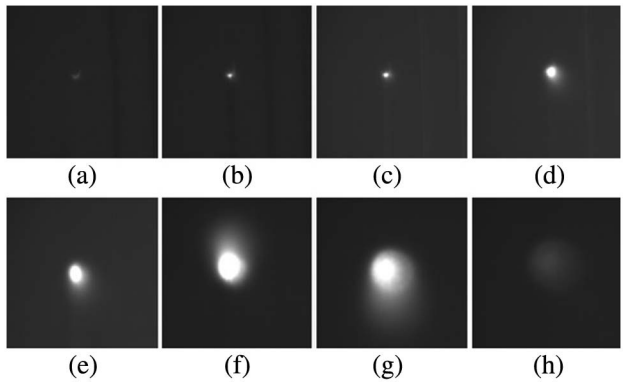

Fig. 3. Pictures of different focusing taken over water-white glass substrate (20× microscope objective, laser beam power of 9.5 mW, and writing speed of 400 μm/s). (a) Focus under surface, (b) and (c) focus on surface, and (d)–(h) focus above the surface.

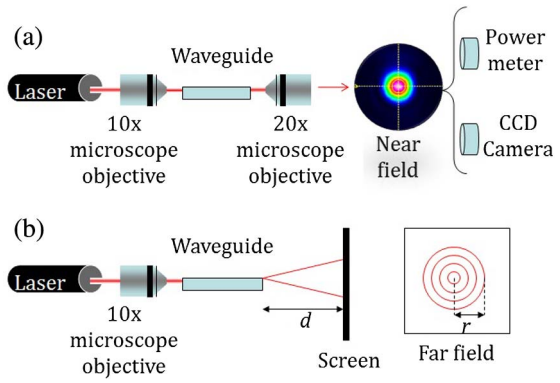

Fig. 4. Schematic representation of the experimental setup used to: (a) measure power at input and output of the waveguides, laser beam waist, and waveguide mode dimensions and (b) measure d and r to calculate NA.

The change in refractive index, (Δn), was measured through the method described in [21]. This requires Eqs. (2) and (3) to calculate Δn, where NA is the numerical aperture, d is the distance between the waveguide exit plane and the screen on which the far-field pattern is seen, r is the external radius of the circular fringes, and n is the bulk substrate refractive index:

$$\mathrm{NA} = \sin\left(\arctan\left(\frac{r}{d}\right)\right), \tag{2}$$

$$\mathrm{NA} = \sqrt{2n\Delta n}. \tag{3}$$

To determine the NA, the 20 × microscope objective was removed and the guided light was projected onto a screen located at different distances (100 and 157 cm), as shown in Fig 4 (b). To get the value for each guide five measures were taken and averaged. The far-field interference pattern in the form of rings could be observed on the screen.

The energy transfer is a prime consideration in determining the efficacy of the laser writing process; therefore the energy dose (D) was calculated [21,22]. This method requires Eq. (4) to calculate D, where E_L is the laser pulse energy, R the laser's repetition rate, A the focused spot area, and v the writing speed. For every waveguide, the change in refractive index was measured and plotted against the energy dose used in its manufacture:

$$D = \frac{E_L R}{Av}. \tag{4}$$

3. RESULTS AND DISCUSSION

Regarding type I buried waveguides, the optimum energy dose range where waveguiding was obtained was found between 0.14 and 0.62 μJ/μm^3. Below 0.14 μJ/μm^3 no measurable change in refractive index could be observed. At an energy dose higher than 0.62 μJ/μm^3 the refractive index decreases and above 1.04 μJ/μm^3 damage was observed. The optimum writing speed range for maximum index contrast was found between 100 and 400 μm/s. At speeds between 400 and 1000 μm/s, the quality of the waveguide is not good and by higher speeds dotted structures were seen [16]. On the other hand, at lower speeds damage was generated. Waveguides that supported single-mode and two-mode propagation at 633 nm were fabricated; waveguide width, writing depth, refractive index change, numerical aperture, and guided beam profile were measured. To measure the near field, a 30 dB attenuator filter was collocated before the CCD camera. For two different waveguides, the near-field intensity distribution of a single- and two-mode propagation is shown in Fig. 5. This is in agreement with V parameter calculations, from which monomode behavior is obtained for a maximum waveguide width/thickness of about 10–12 μm for the NA achieved in the fabricated waveguides. The waveguides were written at 50 μm depth. It is worth noting that the profile is very close to a circular shape. In terms of the refractive index distribution for the fabricated buried waveguides, these exhibit a rectangular cross section of ∼10–16 μm^2 in both horizontal and vertical directions with a refractive index increase of ∼5–7 × 10^{-4}, and are surrounded by the glass substrate, which has a refractive index of 1.51.

Regarding ridge waveguides, the optimum energy dose range where waveguiding was obtained was found between 2.04 and 31.97 μJ/μm^3. Below 2.04 μJ/μm^3 engraving is not deep enough and it does not work as a border of the waveguide core. At energy doses higher than 31.97 μJ/μm^3 borders are perfectly written, but the region between the borders receives very high energy and is damaged. In this case the optimum writing speed range also depends on the power beam, the separation between every written track, and the microscope objective. Therefore it is advisable to work between 20 and 300 μm/s [23]. Figure 6 shows different views and the near-field intensity distribution for two different monomodal waveguides. In terms of the refractive index distribution, the ridge waveguides show a rectangular cross section of ∼10–15 × 15–20 μm^2 with a refractive index increase of ∼5.5–9.5 × 10^{-4} with respect to the glass, bordered on the top by air and below by the substrate, whereas the sides of the ridges comprise the lower refractive index laser-written regions.

Figure 7 shows the variation of the refractive index as a function of energy dose for both waveguide types. Regarding buried waveguides the trending line (second-order polynomial) indicates that the refractive index variation increases with an energy dose from 0.14 μJ/μm^3 up to about 0.7 μJ/μm^3; after this

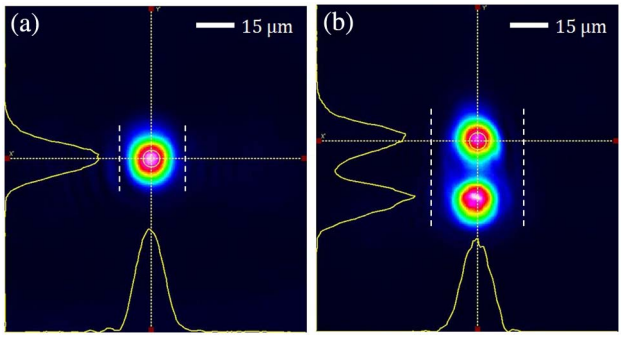

Fig. 5. Near-field intensity distribution of: (a) a single-mode waveguide (corresponding writing parameters in Table 1, number 16); (b) a two-mode waveguide (Table 1, number 19). The writing tracks are marked as white dashed lines.

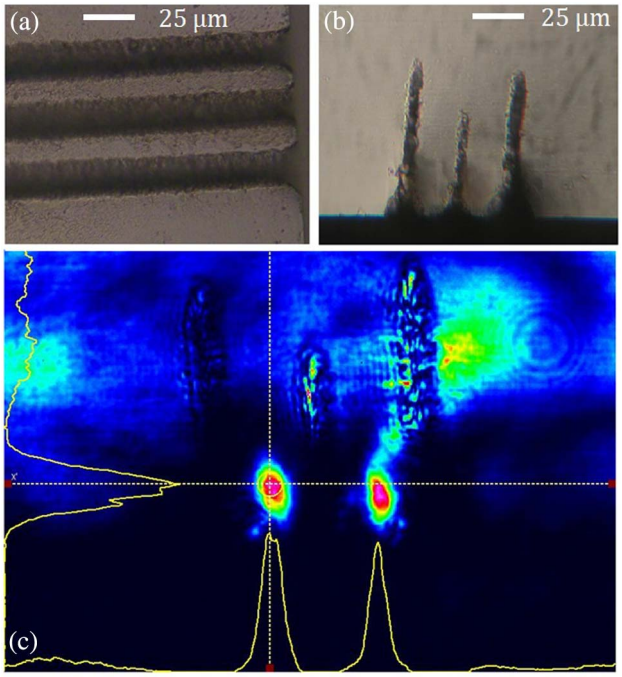

Fig. 6. Ridge waveguides: (a) top view (50 × observation); (b) cross-section view (50 ×); and (c) single-mode near-field intensity distribution of two different ridge waveguides (corresponding writing parameters in Table 1, number 26).

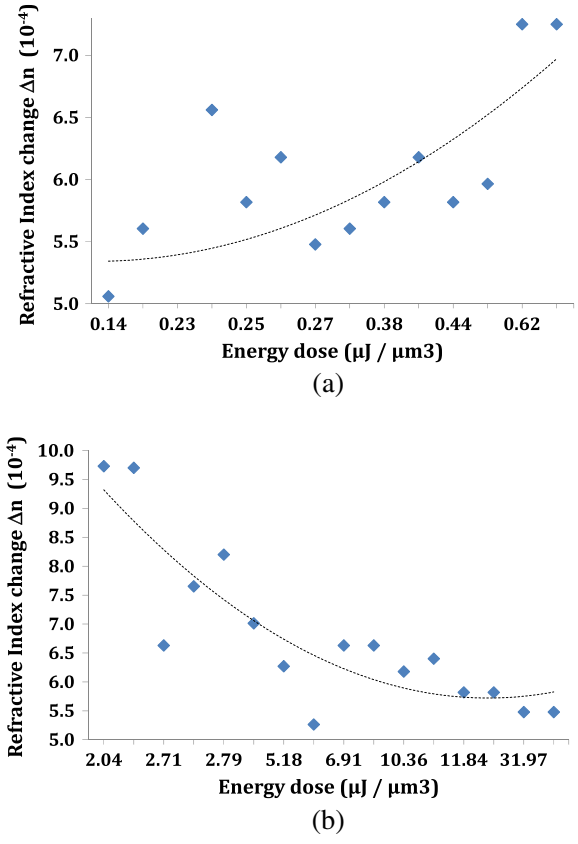

Fig. 7. Variation of the refractive index as a function of energy dose. (a) Buried waveguides and (b) ridge waveguides.

point the refractive index change decreases. This energy dose fabrication window shows close energy values but lower than those presented in [21] and higher refractive index changes. This is expected because the transformation temperature value (T_g) is lower in water-white glass compared with BK7 glass [24]; therefore, lower energy is required to fabricate a waveguide with a similar refractive index change.

Regarding ridge waveguides, the trending line (second-order polynomial) indicates that the refractive index decreases from the first value onward (2.04 μJ/μm^3). This happens because in this case more energy was applied to create the tracks and the area that lies between both engravings receives more energy from around as the engraving is deeper, up to the point that the core region could be damaged.

Figure 8 shows α values of fabricated waveguides as a function of energy dose. The laser writing parameters are shown in Table 1; in all cases the repetition rate was 1 kHz. The triangle symbols in Fig. 8 represent the waveguides based on the type I structure and the square symbols represent the waveguides based on the type II structure. According to these results, the average propagation losses for fabricated waveguides based on the type I structure are around 1.6 dB/cm, highlighting two waveguides with α values of 0.7 dB/cm, which in our opinion is remarkable considering the kind of glass used in the fabrication (Corning 2947B microscope slides).

Regarding ridge waveguides, the average propagation loss is around 5.6 dB/cm. This lower quality is due to the rough sidewalls produced by the fs laser ablation, which introduces considerable losses [11]. There are subsequent treatments to improve the waveguide quality, which are discussed in [25]. Figure 9(a) shows scanning electron microscope (SEM) micrographs of written tracks to define a ridge waveguide. In Fig. 9(b), detail of the formation of microscale/nanoscale features over sidewalls can be seen. Structures are smaller than 1 μm. Similar feature formation was seen in [26] where an analysis of fs laser-induced nanostructures was realized in soda-lime glass.

Comparing the results of both types of waveguide structures in terms of energy dose, it is possible to assert that to fabricate

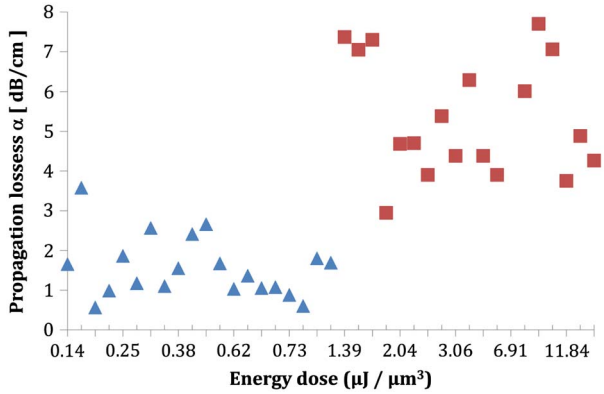

Fig. 8. α values of fabricated waveguides as a function of energy dose. Triangle symbols represent waveguides based on the type I structure and square symbols represent waveguides based on the type II structure.

Table 1. Laser Writing Parameters of Fabricated Waveguides[a]

Waveguide		Incident Energy	Area	Writing speed	Energy dose
Type	#	[μJ]	[μm²]	[μm/s]	μJ/μm³
Buried type I	1	9	158.37	400	0.14
	2	9	150.66	400	0.15
	3	15	165.13	400	0.23
	4	9	188.69	200	0.24
	5	15	150.66	400	0.25
	6	9	112.16	300	0.27
	7	9	112.16	300	0.27
	8	9	165.13	200	0.27
	9	9	158.37	150	0.38
	10	9	89.08	250	0.40
	11	9	139.85	150	0.44
	12	9	73.90	250	0.49
	13	8.6	55.42	250	0.62
	14	8.6	55.42	250	0.62
	15	9	130.70	100	0.69
	16	9	124.69	100	0.72
	17	8.6	47.17	250	0.73
	18	8.6	39.59	250	0.87
	19	9	158.37	50	1.14
	20	9	158.37	50	1.14
Buried type II	21	14	50.27	200	1.39
	22	14	50.27	150	1.86
	23	14	50.27	150	1.86
	24	6.2	20.27	150	2.04
	25	6.2	20.27	150	2.04
	26	5.5	20.27	100	2.71
	27	5.5	20.27	100	2.71
	28	14	50.27	100	2.79
	29	6.2	20.27	100	3.06
	30	21	20.27	200	5.18
	31	24.3	45.60	100	5.33
	32	21	20.27	150	6.91
	33	21	20.27	150	6.91
	34	21	20.27	100	10.36
	35	21	20.27	100	10.36
	36	24	20.27	100	11.84
	37	24	20.27	100	11.84
	38	24.3	5.07	150	31.97
	39	24.3	5.07	150	31.97

[a]These are organized with ascending energy dose values.

waveguides based on the type I structure a lower energy dose is necessary, exhibiting lower losses than those of type II waveguides. Comparing our results with those found in the literature, waveguides with lower or similar values of propagation losses at 633 nm are reported; however, these were manufactured using BK7 glass as a substrate. For instance, [15] states measuring losses of 0.04 dB/cm. Additionally in [21] and [16] values of 0.5 dB/cm and 0.7 dB/cm are reported, respectively. Also, in [17] values of 0.7 dB/cm were measured using a SF10 glass as a substrate. In summary, the substrates used in the previous examples correspond to optical quality glasses. The contribution of our work lies in demonstrating that it is possible to manufacture waveguides with propagation losses lower than 1 dB/cm using glass of lower optical quality as a substrate but very affordable and easily manufactured.

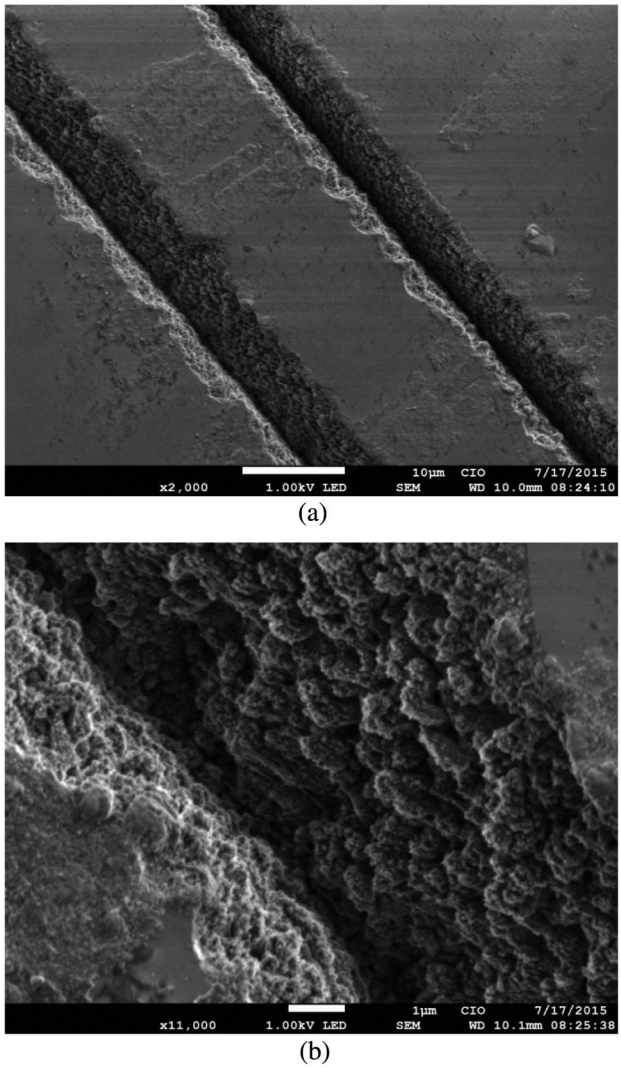

Fig. 9. SEM micrographs of the written tracks of ridge waveguides. (a) Two written tracks (the scale is 10 μm) and (b) detail of one of the sidewall tracks (the scale is 1 μm).

4. CONCLUSIONS

Energy dose ranges were defined for fabricating directly written waveguides based on the type I structure and ablated ridge waveguides based on the type II structure using Corning 2947B microscope glass slides as a substrate. The energy values and range necessary to fabricate type I waveguides are smaller in comparison with those for type II. Although the change in refractive index is higher in type II waveguides than in type I ones, the roughness in the sidewalls that conformed the core border introduces losses and degrades the waveguide quality. Nonetheless, type II structures are important in our research because we will use them in the fabrication of an optochemical sensing device. Therefore, these waveguides will be subjected to a postablation treatment to remove the roughness and improve their quality.

The quality of the directly written waveguides is high, achieving various buried waveguides with α values around 1 dB/cm and even two waveguides with values of 0.7 dB/cm.

This is remarkable considering the kind of substrate used for the fabrication. Additionally, the profile of all the directly written waveguides is symmetric and very close to a circular shape. The results show that the fabricated waveguides are promising for the development of integrated devices.

Funding. Centro de Investigaciones en Óptica (CIO).

Acknowledgment. The authors acknowledge the technical support of Cristóbal García Zavala.

REFERENCES

1. S. L. Li, Y. KaiYe, and M. W. Wang, "Femtosecond laser written channel optical waveguide in Nd:YAG crystal,"Opt. Laser Technol. **58**, 89–93 (2014).
2. K. M. Davis, K. Miura, N. Sugimoto, and K. Hirao, "Writing waveguides in glass with a femtosecond laser," Opt. Lett. **21**, 1729–1731 (1996).
3. R. R. Gattass, L. R. Cerami, and E. Mazur, "Micromachining of bulk glass with bursts of femtosecond laser pulses at variable repetition rates," Opt. Express **14**, 5279–5284 (2006).
4. Ch. B. Schaffer, A. Brodeur, J. F. García, and E. Mazur, "Micromachining bulk glass by use of femtosecond laser pulses with nanojoule energy," Opt. Lett. **26**, 93–95 (2001).
5. L. Tong, R. R. Gattass, I. Maxwell, J. B. Ashcom, and E. Mazur, "Optical loss measurements in femtosecond laser written waveguides in glass," Opt. Commun. **259**, 626–630 (2006).
6. R. R. Gattass, "Femtosecond-laser interactions with transparent materials: applications in micromachining and supercontinuum generation," Ph.D. thesis (Harvard University Cambridge, 2006).
7. H. Huang, L. Yang, and J. Liu, "Femtosecond fiber laser direct writing of optical waveguide in glasses," Proc. SPIE **8164**, 81640B (2011).
8. S. M. Eaton, H. Zhang, P. R. Herman, F. Yoshino, L. Shah, J. Bovatsek, and A. Y. Arai, "Heat accumulation effects in femtosecond laser written waveguides with variable repetition rate," Opt. Express **13**, 4708–4716 (2005).
9. K. Minoshima, A. M. Kowalevicz, I. Hartl, E. P. Ippen, and J. G. Fujimoto, "Photonic device fabrication in glass by use of nonlinear materials processing with a femtosecond laser oscillator," Opt. Lett. **26**, 1516–1518 (2001).
10. S. Gross, M. Dubov, and M. J. Withford, "On the use of the Type I and II scheme for classifying ultrafast laser direct-write photonics," Opt. Express **23**, 7767–7770 (2015).
11. F. Chen and J. R. Vázquez de Aldana, "Optical waveguides in crystalline dielectric materials produced by femtosecond-laser micromachining," Laser Photonics Rev. **8**, 251–275 (2014).
12. J. Cugat, A. Ruiz de la Cruz, R. Solé, A. Ferrer, J. J. Carvajal, X. Mateos, J. Massons, J. Solís, G. Lifante, F. Díaz, and M. Aguiló, "Femtosecond-laser microstructuring of ribs on active (Yb,Nb):RTP/RTP planar waveguides," J. Lightwave Technol. **31**, 385–390 (2013).
13. J. Gottmann, D. Wortmann, I. Vasilief, L. Moiseev, and D. Ganser, "Manufacturing of Nd:$Gd_3Ga_5O_{12}$ ridge waveguide lasers by pulsed laser deposition and ultrafast laser micromachining," Appl. Surf. Sci. **254**, 1105–1110 (2007).
14. Y. Cheng, J. Lv, S. Akhmadaliev, I. Hernández-Palmero, C. Romero, J. R. Vázquez de Aldana, S. Zhou, and F. Chen, "Optical ridge waveguides in Yb:YAG laser crystal produced by combination of swift carbon ion irradiation and femtosecond laser ablation," Opt. Laser Technol. **72**, 100–103 (2015).
15. J. A. Dharmadhikari, K. Pradyna, A. Bhatnagar, D. Mathur, and A. K. Dharmadhikari, "Effect of chirp on the index contrast of waveguides written in BK7 glass with ultrashort laser pulses," Opt. Commun. **287**, 122–127 (2013).
16. J. Thomas, R. Bernard, K. Alti, A. K. Dharmadhikari, J. A. Dharmadhikari, A. Bhatnagar, C. Santhosh, and D. Mathur, "Pattern formation in transparent media using ultrashort laser pulses," Opt. Commun. **304**, 29–38 (2013).
17. J. Bai, X. Long, X. Liu, G. Huo, W. Zhao, R. Stoian, R. Hui, and G. Cheng, "Embedded optical waveguides fabricated in SF10 glass by low-repetition-rate ultrafast laser," Appl. Opt. **52**, 7288–7294 (2013).
18. Abrisa technologies, "Specialty glass materials products & specifications 04/14," 9–10 (2014).
19. H. Lazcano, J. L. Flores, A. Blanco, A. Hernández, R. Nieto, J. L. Martínez, R. A. Torres, G. V. Vázquez, and J. L. Hurtado, "High quality polishing procedure of glass substrates: application in integrated optics," in *ISEM SOI Conference Proceedings of the Society for Experimental Mechanics Series* (Springer International, 2015).
20. J. F. Bourhis, "Fibre to waveguide connection in glass integrated optics and optical fiber devices," in *Critical Reviews of Optical Science and Technology* (SPIE Optical Engineering, 1994), Vol. **CR53**, pp. 335–366.
21. J. A. Dharmadhikari, A. K. Dharmadhikari, A. Bhatnagar, A. Mallik, P. Ch. Singh, R. K. Dhaman, K. Chalapathi, and D. Mathur, "Writing low-loss waveguides in borosilicate (BK7) glass with a low-repetition-rate femtosecond laser," Opt. Commun. **284**, 630–634 (2011).
22. A. Zoubir, M. Richardson, L. Canioni, A. Brocas, and L. Sarger, "Optical properties of infrared femtosecond laser-modified fused silica and application to waveguide fabrication," J. Opt. Soc. Am. B **22**, 2138–2143 (2005).
23. H. E. Lazcano, R. A. Torres, and G. V. Vázquez, "Design and construction of optical waveguides through femtosecond laser micromachining," in *Proceedings of the Mexican Optics and Photonics Meeting (MOPM)* (2015).
24. Schott optical glass pocket catalog, January 2014, rows 94–135.
25. R. Degl'Innocenti, S. Reidt, A. Guarino, D. Rezzonico, G. Poberaj, and P. Gunter, "Micromachining of ridge optical waveguides on top of He^+ implanted β-BaB_2O_4β-BaB_2O_4 crystals by femtosecond laser ablation," J. Appl. Phys. **100**, 113121 (2006).
26. Md. Sh. Ahsan and M. S. Lee, "Femtosecond laser induced nanostructures in soda-lime glass," J. Laser Micro. Nanoeng. **7**, 202–207 (2012).